Cardiovascular Drugs and Therapy (2021) 35:927–938
https://doi.org/10.1007/s10557-020-07014-9

ORIGINAL ARTICLE

Prolonged-release pirfenidone prevents obesity-induced cardiac steatosis and fibrosis in a mouse NASH model

Jorge Gutiérrez-Cuevas[1] · Ana Sandoval-Rodríguez[1] · Hugo Christian Monroy-Ramírez[1] · Monica Vazquez-Del Mercado[2] · Arturo Santos-García[3] · Juan Armendáriz-Borunda[1,3]

Published online: 3 July 2020

Abstract

Purpose Obesity is associated with systemic insulin resistance and cardiac hypertrophy with fibrosis. Peroxisome proliferator-activated receptors (PPARs) regulate carbohydrate and lipid metabolism, improving insulin sensitivity, triglyceride levels, inflammation, and oxidative stress. We previously demonstrated that prolonged-release pirfenidone (PR-PFD) is an agonistic ligand for Pparα with anti-inflammatory and anti-fibrotic effects, and might be a promising drug for cardiac diseases-treatment. Here, we investigated the effects of PR-PFD in ventricular tissue of mice with nonalcoholic steatohepatitis (NASH) and obesity induced by high-fat/high-carbohydrate (HFHC) diet.

Methods Five male C57BL/6 J mice were fed with normal diet (ND) and ten with HFHC diet for 16 weeks; at 8 weeks of feeding, five mice with HFHC diet were administered PR-PFD (350 mg/kg/day) mixed with HFHC diet.

Result Systemic insulin resistance, heart weight/body weight ratio, myocardial steatosis with inflammatory foci, hypertrophy, and fibrosis were prevented by PR-PFD. In addition, HFHC mice showed significantly increased desmin, Tgfβ1, Timp1, collagen I (Col I), collagen III (Col III), TNF-α, and Nrf2 mRNA levels, including α-SMA, NF-kB, Nrf2, troponin I, Acox1, Cpt1A, and Lxrα protein levels compared with the ND ventricular tissues. Mechanistically, HFHC mice with PR-PFD treatment significantly decreased these genes overexpressed by HFHC diet. Furthermore, PR-PFD overexpressed the Pgc1a mRNA levels and Pparα, Pparγ, Acox1, and Cpt1A protein levels.

Conclusions The results suggest that PR-PFD could be a promising drug for the prevention and treatment of cardiac steatosis and fibrosis induced by obesity.

Keywords High-fat/high-carbohydrate diet · Cardiac steatosis and fibrosis · Male C57BL/6 J mice · Prolonged-release pirfenidone · PPARs

Introduction

Obesity is a chronic, multifactorial, and largely preventable disease that affects all kind of socioeconomic groups; it is caused by an imbalance between dietary energy consumption relative to energy expenditure. According to latest WHO estimates, in 2016, more than 1.9 billion of people aged 18 years and older were overweight worldwide; and of these over 650 million adults were obese [1, 2]. Globally, this disease is rapidly rising, and is getting increasing attention given its strong association with cardiovascular diseases (CVDs). Hence, there is an increasing demand for new therapies targeted for CVDs. Fatty acids are the main energetic lipids metabolically utilized by the heart, which represent approximately 70% of the heart energy requirements in normal conditions [3].

Electronic supplementary material The online version of this article (https://doi.org/10.1007/s10557-020-07014-9) contains supplementary material, which is available to authorized users.

✉ Juan Armendáriz-Borunda
armdbo@gmail.com

[1] Department of Molecular Biology and Genomics, Institute for Molecular Biology in Medicine and Gene Therapy, University of Guadalajara, CUCS, Guadalajara, Jalisco, México

[2] University of Guadalajara, IIRSME, CUCS, Guadalajara, Jalisco, México

[3] Tecnologico de Monterrey, Campus Guadalajara, Guadalajara, Jalisco, México

However, in pathological situations such as advanced hypertrophy and other cardiomyopathies, cardiac energy metabolism switches from fatty acids to glucose for ATP production [3].

The high-fat/high-carbohydrate (HFHC) diet, commonly known as Western diet, induces obesity, which is associated to metabolic syndrome, type 2 diabetes (T2D), nonalcoholic steatohepatitis (NASH), and CVDs [4, 5]. In male C57BL/6 J mice, the persistent caloric excess provided by HFHC diet increases weight, body fat mass, fasting glucose, insulin resistance, and plasma cholesterol [5]. Buildup of lipids in the heart tissue leads to alterations in cardiac morphology and function due to glucose intolerance, low-grade inflammation, and impaired insulin sensitivity [5–7]. High fat diet (HFD) induces myocardial oxidative stress, defective intracellular signaling, cardiomyocyte hypertrophy, interstitial fibrosis, and dysregulation of genes such as peroxisome proliferator-activated receptors (PPARs), including Pparα and Pparγ [8–11]. Thus, these pathological alterations, mainly interstitial fibrosis, may cause myocardial stiffness [11]. PPARs are master regulators of lipid and carbohydrate metabolism, enhancement of insulin sensitivity, and inhibition of inflammation and oxidative stress [12].

Pirfenidone (PFD) is a drug with anti-inflammatory, antioxidant, and anti-fibrotic effects in various tissues such as the lung, the liver, the heart, and other organs [13–16]. We have recently shown that prolonged-release pirfenidone (PR-PFD) is an agonistic ligand for Pparα and decreases hepatic steatosis and fibrosis [17]. Nonetheless, little is known concerning the role of pirfenidone on cardiac steatosis and fibrosis induced by a HFHC diet. Therefore, we assess the effect of PR-PFD in order to ameliorate triglyceride content and prevent HFHC-induced myocardial fibrosis using male C57BL/6 J mice that develop obesity and a NASH phenotype [5]. We started to feed 5-week-old mice with HFHC diet for 16 weeks, and at 8 weeks of feeding, mice were intervened with PR-PFD treatment. We evaluated genes related to lipid metabolism, inflammation, oxidative stress, and myocardial damage in the ventricular tissue of obese mice. We also analyzed the effect of PR-PFD on the protein expression of transcriptional factors/nuclear receptors Pparα and Pparγ in cardiac tissue of mice fed HFHC diet.

Methods

Animal Care

CUCS Research Committee at the University of Guadalajara approved this study (protocol number: CI-01419). All animal experiments were performed in compliance with the guidelines for the care and use of laboratory animals published by the US National Institutes of Health (NIH, publication No. 85-23, revised 1996). Four-week-old male C57BL/6 J mice weighing between 18-22 g were purchased from the National Polytechnic Institute (Mexico City, Mexico). Mice were housed in polycarbonate cages with a humidity of 40-50% and a temperature of 21-22 °C, including a 12 h light-dark cycle. Animals were provided ad libitum access to food and water. Experiments were done and results were reported in accordance with the ARRIVE guidelines.

Experimental Design

At the age of 5 weeks, animals were randomly assigned into two groups; normal diet (ND, $n = 5$) and high-fat/high-carbohydrate (HFHC, $n = 10$) diet. ND was composed of 18% kcal from fat food (2018S.15-Envigo, Supplement Table S1). HFHC diet consisted of 60% kcal from fat food (TD.06414-Envigo, Supplement Table S1) and drinking water with 42 g/L of carbohydrates (55% fructose and 45% sucrose) [5]. At the end of the eighth week, five HFHC mice were treated with approximately 350 mg/kg/day of PR-PFD (Cell Pharma S.A. de C.V.) mixed with food (HFHC + PR-PFD, $n = 5$); the dose was chosen according to the reported in a mouse model of NASH [18]. Another set of animals was subjected to HFHC diet ($n = 12$) and sacrificed by groups ($n = 3$) at 4, 8, 12, and 16 weeks to monitor cardiac steatosis and fibrosis development.

Food and Water Intake Measurement

Food and water consumption were calculated by subtracting the amount of food and water left, three times for week. Mice groups ($n = 5$ or $n = 3$) were housed per cage, respectively, and food and water intake values were divided by the number of animals per cage. Energy intakes were calculated based on 3.1 kcal/g for the ND and 5.1 kcal/g for HFHC groups. Carbohydrate intakes in water were considered as well.

Insulin Tolerance Test

Insulin tolerance test (ITT) was performed in mice using tail blood. After fasting for 4 h, basal glucose was determined. A total of 100 μL saline solution containing a dose of 0,025 IU/mouse of human-recombinant short-acting insulin (Humulin R, Lilly) was administered intraperitoneally. Glucose levels were determined at 30, 60, and 90 minutes with a glucometer (One Touch Ultra, LifeScan Inc.). Area under the curve (AUC) was calculated.

Heart and Liver Dissection

Mice were anesthetized with tiletamine/zolazepam (15 mg/kg/bw, Zoletil® 50, Virbac); the hearts and livers were rapidly isolated. Previously, mice heart was perfused through left ventricular using a syringe with 5 mL of ice cold PBS. Auricles

were removed and ventricles were sliced in four sections; one was fixed in 4% paraformaldehyde (0.1 M PBS, pH 7.4) and embedded in paraffin; other was immersed in Tissue-Tek® OCT. The other two ventricle portions were used to extract protein and total RNA, respectively. Sliced sections of liver were fixed in 4% paraformaldehyde (0.1 M PBS, pH 7.4), and embedded in paraffin.

Oil Red O and Hematoxylin-Eosin (H&E) Staining

For oil red O (ORO), OCT frozen blocks of cardiac tissue were cut in 8 μm-thick slices and fixed with ice-cold 10% paraformaldehyde, washed with distilled water, and dried for 2 minutes. Isopropanol (60%) was added for 60 seconds, stained with ORO for 15 minutes followed by adding 60% isopropanol for 30 seconds, washed three times with distilled water, and counterstained with Harris' hematoxylin for 1 min.

Serial ventricular sections of 5 μm were cut and processed according to standard hematoxylin-eosin (H&E) staining, and inflammatory foci were explored in ventricular and liver tissue. Digital images (Olympus BX51) of 7 random fields were captured from each mouse heart. Lipid content per tissue area within each field and cardiomyocyte size (quantitation of 350 cells per mice group) was determined using ImageJ.

Masson Staining Morphometric Analysis

Masson's trichrome and picrosirius red staining were made according to standard procedures (Sigma-Aldrich). Fibrotic area in the total field area was assessed in 7 representative images per heart, using ImageJ.

Immunohistochemistry

After deparaffinization and rehydration, ventricular tissues were treated with 3% H2O2 in absolute methanol for 20 min. Sections were incubated overnight at 4 °C with monoclonal antibody rabbit anti-α-SMA (Supplement Table S2), then detected with avidin-conjugated secondary antibodies, and visualized with a Vectastain kit, PK-8800 (Vector Laboratories) and diaminobenzidine (Sigma-Aldrich). Sections were lightly counterstained with hematoxylin, before being dehydrated and mounted. The antigen retrieval was performed in water bath set to 99 °C for 25 min in Tris-EDTA buffer, pH 9.0. For quantification, 7 random fields of ventricular areas were evaluated. Staining intensity of α-SMA was determined using ImageJ.

RNA Isolation and RT-qPCR

Total RNA from ventricular tissue was isolated with Trizol reagent (Invitrogen) according to the manufacturer's instructions, and quantified using NanoDrop spectrophotometer (Thermo Fisher Scientific). Two micrograms of total RNA was reverse-transcribed using 690 ng random primers, 0.72 mM deoxynucleotide triphosphate (dNTP) mix, 1x first-strand buffer, 3.6 mM dithiothreitol (DTT), 5 U of RNAase inhibitor, and 260 U Moloney Murine Leukemia Virus (M-MLV) reverse transcriptase (Invitrogen) in a 50 μL reaction volume, following manufacturer's directions. Each qPCR was carried out using 1 μL of cDNA, 1x Universal PCR Master Mix, and 1x specific Taqman primer/probe (Supplement Table S3). qPCR reactions were performed on the LightCycler 96 Instrument (Roche Molecular Systems). All data were run in triplicate, normalized according to Gapdh and 18S levels, and analyzed using $2^{-\Delta\Delta Ct}$ method.

Western Blot Analysis

Snap-frozen ventricular tissue was homogenized in RIPA buffer; 40 μg of total cardiac protein was resolved per lane in 12% SDS-PAGE gel and transferred to PVDF membrane (Bio-Rad Laboratories). Membranes were incubated with 3% nonfat dry milk in Tris-buffered saline containing 0.1% Tween 20 at room temperature for 1 h. Membranes were immunoblotted with specific primary antibodies (Supplement Table S2). Primary antibodies were used at 1:1000 dilution and incubated overnight at 4 °C. Subsequently, peroxidase-conjugated secondary antibody (Roche) was used at 1:12000 dilution for 1 h at room temperature. Protein bands were detected using BM Chemiluminescence Western Blotting Kit (Roche Applied Science), and analyzed for density through ChemiDoc XRS+ with the Image Lab software (Bio-Rad Laboratories). All western blots were performed in triplicate samples. β-actin was used as constitutive protein.

Data Analysis

Data were tested for normal distribution using the Shapiro-Wilk test and Kolmogorov-Smirnov test. The error bars of data are presented as median ± quartile for Mann-Whitney *U* test, which was performed on data that were not normally distributed. Statistical significance was determined for parametric data with Welch's *t* test for two groups, and one-way ANOVA analysis of variance followed by Tukey's post hoc analysis. The error bars of data are expressed as mean ± standard error of the mean (SEM). Statistical analyses were performed using SPSS (IBM Corp., version 24). *P* values less than 0.05 were considered significant. We determined power analysis of data by the program G3*Power 3.1.9.2; we calculated effect size and α was 0.05; power values were 0.76–1.

Results

Animal Characteristics and Metabolic Parameters

Two groups of male C57BL/6 J mice were subjected to ND or HFHC diet during 16 weeks; while one mice group was fed with HFHC diet for 8 weeks, and then treated with PR-PFD (Fig. 1a).

All HFHC mice showed an increase in visceral fat accumulation and heart weight gain (Fig. 1b). Histological examination of liver sections from mice fed HFHC diet for 16 weeks exhibited development of steatosis with hepatocytes ballooning, including inflammation and fibrosis (Fig. 1c).

Statistically significant changes of caloric intake in the HFHC group were noted when they were compared with ND group (Fig. 2 a and b, $P < 0.001$). Table 1 describes the characteristics of animal groups. HFHC mice developed hyperglycemia (198 ± 27.57 mg/dL) and insulin sensitivity alterations (18.09 ± 3.38) compared with the ND mice (111 ± 12.01 mg/dL and 9.66 ± 1.25, respectively; $P < 0.01$). PR-PFD treatment in HFHC mice improved insulin sensitivity ($P < 0.05$ vs. HFHC), which was analyzed by AUC. HFHC group showed an increase in fat accumulation and a significant ($P < 0.001$) increase body weight compared with the ND mice (49.25 ± 4.72 g vs. 27.98 ± 0.94 g, respectively). In HFHC animals treated with PR-PFD, body weight diminished to 40.33 ± 5.65 g ($P < 0.05$ vs. HFHC). ND mice showed a HW/BW ratio of 5.95 ± 0.23 mg/g, and HFHC diet decreased significantly HW/BW ratio (3.69 ± 0.40 mg/g; $P < 0.001$ vs. ND), but it was recuperated to 4.97 ± 0.63 mg/g by the treatment with PR-PFD (Table 1, $P < 0.01$ vs. HFHC).

PR-PFD Attenuates HFHC-Induced Cardiac Lipid Accumulation

Histologic analyses were used to assess the myocardial lipid content in C57BL/6 J mice fed HFHC diet. Oil red O staining showed that HFHC diet significantly increased by 1.8-fold of content of small lipid droplets in myocytes (Fig. 3 c and e, $P < 0.001$ vs. ND). Lipid accumulation was gradually increased since the fourth week up to the sixteenth week (Fig. 3 a and d, $P < 0.05$). Noteworthy, excess of big lipid droplets in some tissue areas were common (Fig. 3b, 16 weeks). Oil red O staining showed since the twelfth week that droplets of lipid were more abundant in left ventricle than in right ventricle of the hearts from HFHC-induced obese mice (Fig 3b, 12 weeks), indicating a steady accumulation of lipids on heart tissue following initiation of the HFHC diet. PR-PFD in HFHC mice reduced to 1.4-fold the lipid levels (Fig 3 c and e, $P < 0.05$ vs. HFHC).

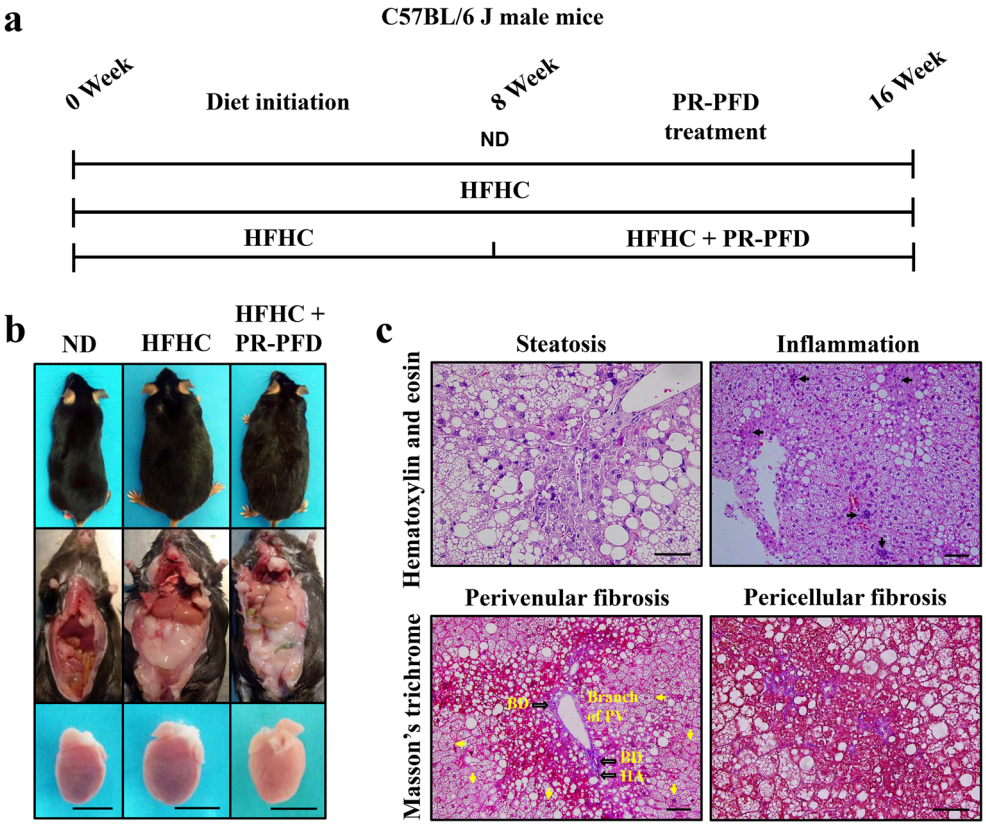

Fig. 1 HFHC diet leads to obesity, visceral fat accumulation, and NASH. **a** Experimental design that shows the weeks of diet and PR-PFD treatment. **b** Macroscopic comparison of body weight, abdominal cavity terminal dissection of visceral adipose tissue showing the liver, and the heart's size (scale bar: 5 mm). **c** The liver of HFHC diet showing microvesicular and macrovesicular steatosis, scale bar: 150 μm (magnification × 40); some neutrophilic inflammatory foci are indicated in black arrows, scale bar: 100 μm (magnification × 20); perivenular fibrosis and ballooning hepatocytes are indicated by yellow arrows; scale bar: 100 μm (magnification × 20). Pericellular fibrosis with scale bar: 150 μm (magnification × 40). Pictures illustrate representative mice per group ($n = 5$). PV, portal vein; BD, bile duct; HA, hepatic artery

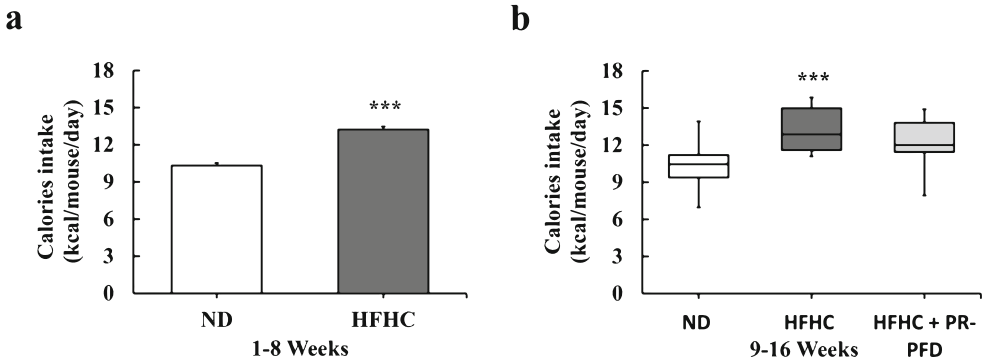

Fig. 2 Average daily caloric intake in mice groups before and during treatment with PR-PFD. **a** Caloric intake measured previous treatment with PR-PFD. For group comparisons (Welch's *t* test), data are expressed as mean ± SEM, *n* = 24/group. **b** Caloric intake measured during treatment with PR-PFD. For group comparisons (Mann-Whitney *U* test), data are expressed as median ± quartile, *n* = 24/group. ***P < 0.001 vs. ND

PR-PFD Protects Mice from Heart Hypertrophy and Inflammation Induced by HFHC Diet

In order to determine the HFHC diet impact on myocardial histology, cardiomyocyte cross-sectional area and neutrophilic inflammatory foci were examined. Heart sections stained with H&E revealed at 16 weeks a significant ($P < 0.001$) increase in the median of cross-sectional area in mice fed HFHC diet compared with those ND mice (222.13 μm^2 vs. 389.79 μm^2, respectively), which indicates cardiomyocyte hypertrophy (Fig. 4 a and b). The median of cardiomyocytes size was reduced to 377.70 μm^2 in mice fed with HFHC and PR-PFD compared with the HFHC mice (Fig 4b, $P < 0.01$).

Next, we examined the presence of neutrophilic inflammatory foci in heart tissue of HFHC mice. Recruitment of several inflammatory foci emerged at the eight week and was more evident at the sixteenth week (Fig. 4 c and d). The inflammatory foci induced in HFHC mice at 16 weeks were remarkably prevented by PR-PFD treatment (Fig. 4d).

Effects of PR-PFD on HFHC-Induced Cardiac Fibrosis

Myocardial fibrosis was analyzed in ventricular tissue, which has been associated to myocardial stiffness. We found in HFHC mice through Masson's trichrome staining a significant increase in the extracellular matrix fiber accumulation; the fibrosis was evident since the eight week up to the sixteenth week with around 12% of the fibrotic area (Fig. 5a–d, $P <$ 0.001 vs. eight week and ND). PR-PFD treatment in HFHC group significantly ($P < 0.001$) declined extracellular matrix fibers to 7% of the fibrotic area compared with that in the HFHC group without PR-PFD treatment (Fig. 5c and d). Fibrosis prevention by PR-PFD treatment was also confirmed by picrosirius red staining, which detects mostly collagen I (Col I) and collagen III (Col III) fibers (Fig. 5e). In order to detect the expression levels of fibrosis-related α-SMA protein, we performed immunohistochemical analysis. The α-SMA protein levels were strongly expressed around blood vessels, and were induced by 6.1-fold in HFHC mice compared with 4.4-fold in the ND mice (Fig. 5 f and g, $P < 0.001$), whereas they were significantly decreased to 4.5-fold by PR-PFD treatment (Fig. 5 f and g, $P < 0.001$ vs. HFHC).

mRNA Levels of Genes Implicated in Cardiac Hypertrophy and Fibrosis Are Modified by PR-PFD

The expression of desmin mRNA levels was significantly increased by 1.46-fold in HFHC mice-cardiac tissue compared with those from ND mice ($P < 0.01$), and PR-PFD treatment in HFHC mice showed a significant reduction to 0.65-fold of the desmin mRNA levels (Fig. 6a, $P < 0.001$ vs. HFHC). We also analyzed in HFHC mice, the mRNA

Table 1 Effects of PR-PFD on HFHC-induced cardiac steatosis and fibrosis. AUC, area under the curve; ND, normal diet; HFHC, high-fat/high-carbohydrate; HFHC + PR-PFD, high-fat/high-carbohydrate plus prolonged-release pirfenidone; PR-PFD, prolonged-release pirfenidone; LW, liver weight; HW, heart weight. Data are expressed as mean ± SEM. For group comparisons (*n* = 5/group), one-way ANOVA followed by Tukey's post hoc analysis. **$P < 0.01$ and ***$P < 0.001$ vs. ND; $^{\#}P <$ 0.05, $^{\#\#}P < 0.01$ vs. HFHC

Group	Dose (mg/kg)	Plasma glucose (mg/dL)	AUC	BW (g)	LW (g)	HW (mg)	HW/BW (mg/g)
ND		111 ± 12.01	9.66 ± 1.25	27.98 ± 0.94	1.32 ± 0.16	166.50 ± 7.77	5.95 ± 0.23
HFHC		198 ± 27.57**	18.09 ± 3.38**	49.25 ± 4.72***	2.04 ± 0.34	180.50 ± 2.89	3.69 ± 0.40***
HFHC+PR-PFD	350	177 ± 9.50	11.73 ± 0.70	40.33 ± 5.65	2.85 ± 0.72	198.00 ± 14.04	4.94 ± 0.63

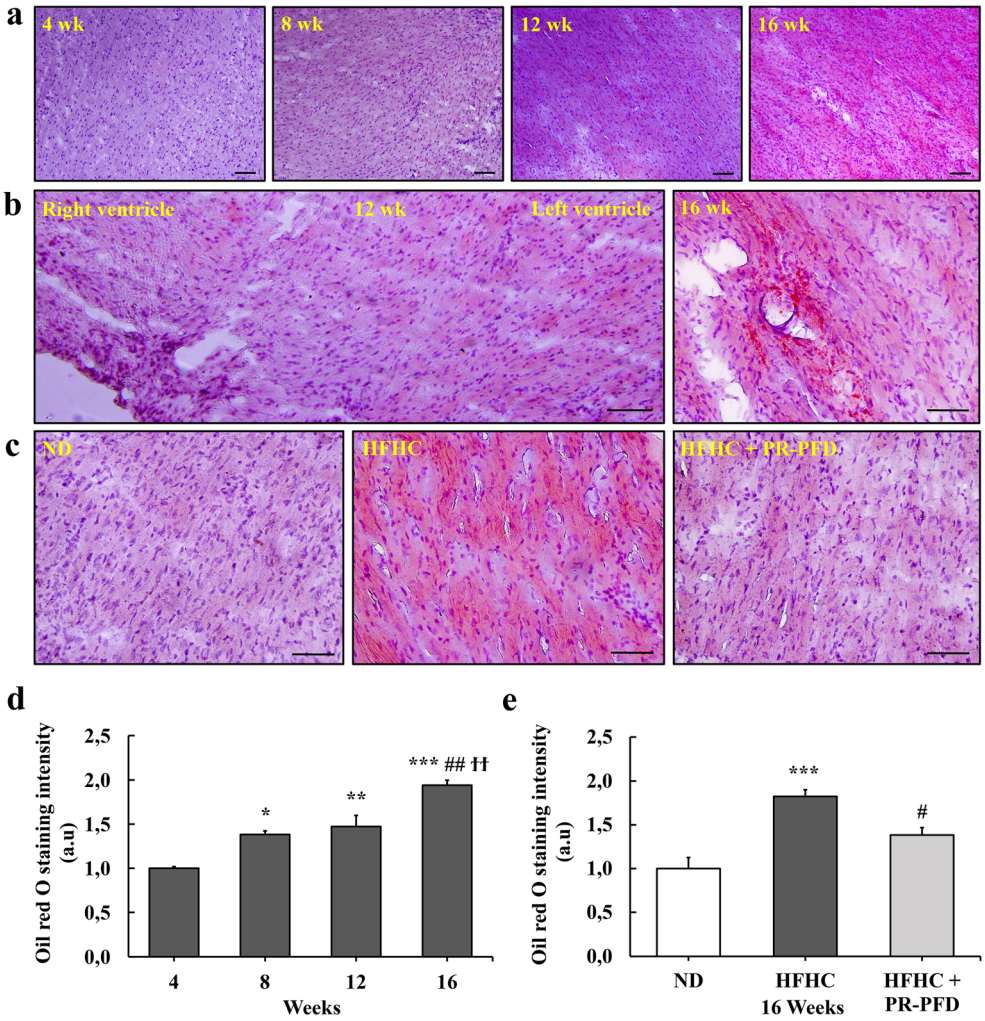

Fig. 3 PR-PFD prevents cardiac lipid accumulation induced by HFHC diet. **a**-**d** Lipid accumulation in frozen heart sections were stained with ORO. Scale bar: 100 μm, magnification × 20 (**a**); 200 μm, magnification × 12 (**b**, 12 weeks) and 150 μm, magnification × 40 (**b**, 16 weeks). **d**, **e** Histograms of lipid content quantified from the fourth week up to the sixteenth week and sixteenth week, respectively. Data are expressed as mean ± SEM. For group comparisons ($n = 35$/group), one-way ANOVA followed by Tukey's post hoc analysis. $^{*}P < 0.05$, $^{**}P < 0.01$, and $^{***}P < 0.001$ vs. 4 weeks or ND; $^{\#\#}P < 0.01$ vs. 8 weeks; $^{\#}P < 0.05$ vs. HFHC and $P < 0.01$ vs. 12 weeks

expression of fibrosis-associated biomarkers, such as Tgfβ1, Timp1, Col I, and Col III, these genes were increased by 1.94-fold, 2.25-fold, 2.15-fold, and 2.72-fold, respectively (Fig. 6a, $P < 0.01$ vs. ND). HFHC mice with PR-PFD showed significantly decreased mRNA levels for Tgfβ1 (1.11-fold), Timp1 (1.29-fold), Col I (1.23-fold), and Col III (1.26-fold) (Fig. 6a, $P < 0.05$ vs. HFHC).

Fibrosis is also associated with persistent inflammation; thus, TNF-α mRNA level expression was analyzed. TNF-α mRNA was significantly elevated by 1.5-fold in HFHC mice compared with the ND mice ($P < 0.01$), while PR-PFD treatment in HFHC mice showed a significant reduction to 0.7-fold of the TNF-α mRNA levels (Fig. 6b, $P < 0.001$ vs. HFHC).

Nrf2 factor is a mediator of antioxidant signaling during inflammation. HFHC diet induced a significant increase of Nrf2 mRNA levels compared with those in ND mice ($P < 0.05$), while PR-PDF treatment was significantly able to prevent Nrf2 gene overexpression (Fig. 6b, $P < 0.001$ vs. HFHC).

Sod1 mRNA levels decreased in HFHC mice compared with those in ND mice, including mice with PR-PDF treatment, but these differences were not statistically significant (Fig 6b).

In addition, Srebp1 and Acox1 mRNA expression was evaluated in order to find the PR-PFD effects on lipid metabolism. Acox1 mRNA levels did not show significant differences between mice groups, and Srebp1 mRNA levels were not significantly changed in animal groups (Fig. 6b).

The mRNA levels of peroxisome proliferator-activated receptor gamma coactivator 1-alpha (Pgc1a), which is a master regulator of mitochondrial biogenesis, were not significantly changed in HFHC mice (decreased by 0.8-fold), while HFHC mice with PR-PDF treatment expressed the Pgc1a mRNA levels to 1.71-fold (Fig. 6b, $P < 0.001$ vs. HFHC).

Determination of Protein Expression Related to Inflammation, Lipid Metabolism, Oxidative Stress, and Myocardial Damage

The HFHC mice-cardiac tissue had significantly elevated by 1.7-fold the NF-kB protein levels compared with those in ND mice, and HFHC mice with PR-PFD significantly reduced to

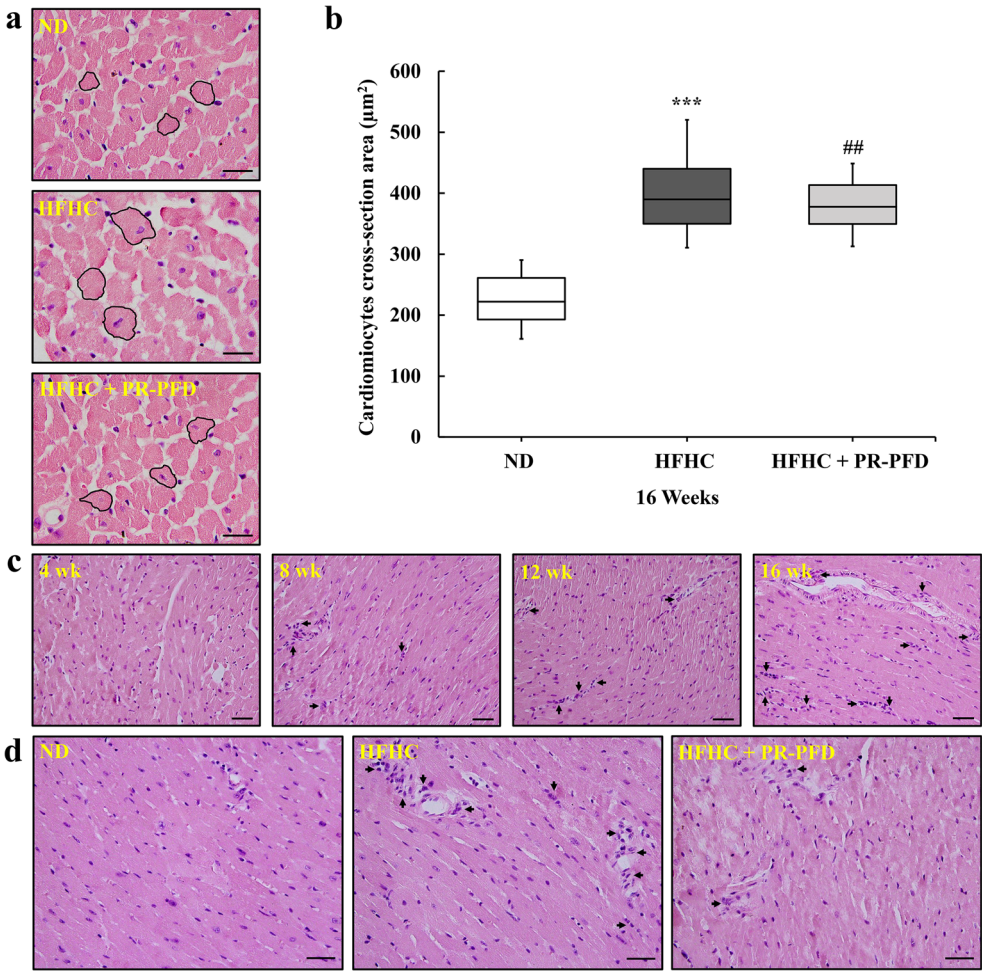

Fig. 4 Representative heart histology features stained with H&E from mice fed with HFHC diet. **a** Micrographs of cardiomyocyte cross-sectional area, depicting cardiomyocyte size of the mice groups at 16 weeks (three cell membranes by photomicrography are limited in black), scale bar: 100 μm, magnification × 100. **b** Histogram showing cardiomyocyte cross-sectional area at 16 weeks. **c**, **d** Heart tissue revealing small neutrophilic inflammatory foci (black arrows) from the fourth week up to the sixteenth week and sixteenth week, respectively; scale bar: 150 μm magnification × 40. Bar graph indicates the median ± quartile, $n = 350$/group. Statistical test was performed by Mann-Whitney U test for group comparisons. $^{***}P < 0.001$ vs. ND; $^{\#\#}P < 0.01$ vs. HFHC

1-fold the NF-kB protein levels compared with HFHC diet (Fig. 7 a and b, $P < 0.01$).

Nrf2 protein levels in the ventricular tissues were significantly upregulated by 1.3-fold in HFHC mice compared with those in ND group, and PR-PFD with HFHC significantly decreased by 0.6-fold the Nrf2 protein levels compared with the HFHC group (Fig. 7 a and b, $P < 0.01$).

We evaluated changes in the expression of troponin I, which is a specific indicator of myocardial damage. Troponin I protein levels were significantly increased by 1.52-fold in HFHC mice compared with ND mice (Fig. 7a and b, $P < 0.01$). Troponin I protein levels were significantly reduced to 0.98-fold in HFHC mice with PR-PFD treatment (Fig. 7 a and b, $P < 0.05$ vs. HFHC), indicating that HFHC diet is harmful to the ventricular tissue.

To explore a possible mechanism by which PR-PFD could help avoid intramyocellular lipid accumulation in cardiac tissue; we focused on the Pparα, Pparγ, Acox1, Cpt1A, Lxrα, and Srebp1 gene expression. Noteworthy, Pparα and Pparγ protein levels were not affected by HFHC diet. Interestingly, Pparα and Pparγ protein levels were significantly increased by 1.3-fold and 1.4-fold upon PR-PFD treatment in HFHC mice (Fig. 7 c and d, $P < 0.01$ vs. HFHC). Acox1 and Cpt1A protein levels were significantly ($P < 0.001$) increased by 0.9-fold and 1.1-fold in HFHC mice compared with the ND mice (0.5-fold and 0.3-fold, respectively), while Acox1 and Cpt1A protein levels were overexpressed to 1.2-fold and 1.5-fold in HFHC mice treated with PR-PFD (Fig. 7 c and d, $P < 0.05$).

Regarding Lxrα protein levels expression, they were significantly increased by 1.5-fold in the ventricular tissue of HFHC mice compared with 0.6-fold of the ND mice (Fig. 7 c and d, $P < 0.01$). However, Lxrα protein levels were slightly decreased in HFHC mice treated with PR-PFD (Fig. 7 c and d).

Srebp1 protein level expression did not show significant differences in HFHC mice compared with ND mice, neither in HFHC mice treated with PR-PFD compared with HFHC mice (Fig. 7 c and d).

Discussion

The HFHC diet used in the present study has been reported to induce obesity, body fat mass, systemic insulin resistance,

fasting glucose, and NASH with fibrosis in male C57BL/6 J mice [5]. We used the same animal model in order to evaluate the impact of HFHC diet on ventricular tissue, and PR-PFD potential effect on the cardiac hypertrophy and fibrosis prevention under lipotoxicity phenotype.

C57BL/6 J mice developed obesity with increases in both total weight and fat mass gain, and an insulin-resistant phenotype due to intake of HFHC diet for 16 weeks [4, 5]. PR-PFD recuperated heart weight to body weight ratio. Wang et al. reported that heart weight/body weight ratio decreased by a chronic high fat diet [8] and reflects the cardiac pathology [19].

The triglyceride accumulation in non-adipose tissues as the myocardium is associated with inflammation, myocardial hypertrophy, and fibrosis in obese conditions [7]. C57BL/6 J mice displayed an increase in diacylglycerols when they were fed with HFD [20], which impaired insulin action through protein kinase C isoform activation [21]. A 2-fold increase cardiac triglyceride content after 7 weeks of HFD has been reported in rats [22]. We observed an increase of myocardial lipids by 1.8-fold after 16 weeks of HFHC-feeding. We demonstrated that PR-PFD treatment decreased lipids in heart of HFHC mice. Furthermore, pirfenidone decreased hepatic lipid accumulation in a mouse model of NASH by polarizing M2 macrophages and by improving systemic insulin sensitivity [23], and our own recent data are consistent with these findings [17].

Obesity leads to myocardial hypertrophy and increases cardiomyocyte size, which has been proposed as the gold standard for diagnosing this pathology [8, 24]. HFD induces myocardial hypertrophy and fibrosis [8]. Cardiac hypertrophy is induced in male C57BL/6 J mice fed with high-fructose diet for 10 weeks, and these mice showed increased of desmin and troponin I protein levels [25]. In addition, C57BL/6 mice fed with HFD for 6 weeks exhibited an increase of plasma cardiac troponin I [26]. We found increased expression of desmin mRNA levels and troponin I protein levels in HFHC mice, and PR-PFD reduced these markers of cardiac hypertrophy. The α-SMA protein expression was found increased in cardiac fibrosis induced by pressure-overloaded hearts and myocardial infarction, and pirfenidone reduced it [15, 16]. Other well-known fibrosis markers are Tgfβ1, Col I, and Col III, including Timp1. For instance, Timp1 deficiency reduces myocardial fibrosis in both models of cardiomyopathy induced by pressure-overloaded hearts and myocardial infarction [27]. Our obese C57BL/6 J mice overexpressed α-SMA protein levels and mRNA levels of Tgfβ1, Timp1, Col I, and Col III in cardiac tissue with fibrosis, and PR-PFD decreased

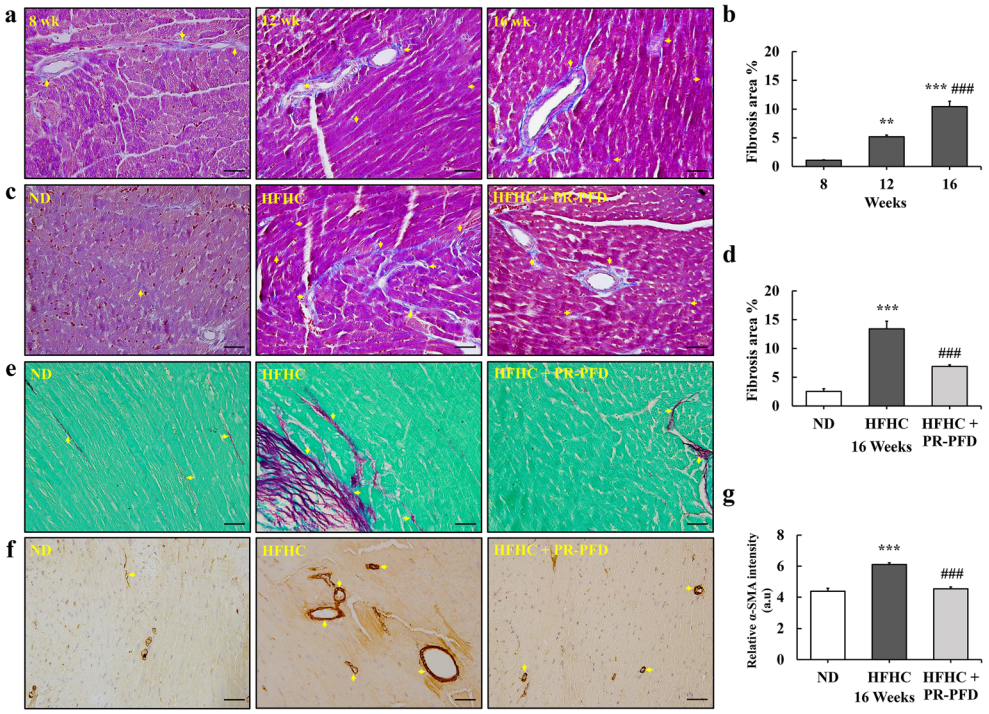

Fig. 5 Histological analysis of PR-PFD effects on HFHC-induced cardiac fibrosis. **a**, **c**, and **e** Representative microphotograph cross sections of heart tissue showing endomysial and perimysial collagen network deposition, stained by Masson's trichrome and picrosirius red. Interstitial fibrosis and perivascular fibrosis are indicated by yellow arrows (**a**, **c**, **e**); collagen fibers appeared at the eight week (**a**). **b**, **d** Histogram representation of collagen deposition of Masson's trichrome stain. **f**, **g** Mice ventricular sections were immunostained with α-SMA, signal mainly around vessels: yellow arrows. Scale bar: 150 μm, magnification × 40. Data are expressed as mean ± SEM. For group comparisons (n = 35/group), one-way ANOVA followed by Tukey's post hoc analysis. $^{**}P < 0.01$ and $^{***}P < 0.001$ vs. the eighth weeks or ND; $^{\#\#\#}P < 0.001$ vs. the twelfth weeks or HFHC

these fibrosis markers in the ventricular tissue of obese mice. Taken together, these results confirm the anti-fibrotic effect of pirfenidone reported in different preclinical and clinical studies [13–16], including mouse models of nonalcoholic steatohepatitis [17, 18, 23].

It is important to note that HFD increases NF-κB activity in mice [28], and NF-κB activation induced by saturated fatty acid coincides with insulin resistance [29]. Mechanistically, TNF-α and free fatty acids activate intracellular kinases in order to induce phosphorylation of IRS proteins, thus attenuating insulin signaling and inducing insulin resistance [30]. Fibrotic cardiomyopathy is characterized by inflammation [11], and Pparα and Pparγ activation attenuates this pathological process through inhibition of NF-κB and TNF-α in cardiac muscle [9, 10]. HFHC mice showed neutrophilic inflammatory foci formation; TNF-α mRNA and NF-κB protein levels increased, and PR-PFD reduced these markers of inflammation, probably due to its anti-inflammatory effects [31], suppression of NF-κB activity [32], and reduction of myocardial triglyceride content.

Pparα has been implicated in the regulation of oxidative stress [10]. In our HFHC mice, no changes statistically significant of Sod1 mRNA levels were found compared with ND mice. In cardiac tissue of C57BL/6 J mice fed with HFD, Sod1 protein levels were expressed similarly to mice fed with control diet [33].

Data of PPAR pathway activation and expression on ventricular hypertrophy are conflicting. In diabetic cardiomyopathy and in chronic exposure to free fat acids, Pparα expression was found reduced [11]. Studies in humans suggest that Pparα expression is not significantly altered in cardiac tissue of T2D patients [11]. We found that Pparα and Pparγ protein levels were not significantly changed in HFHC mice when they were compared with ND mice. Agonists of Pparα and Pparγ reduce free fatty acids and triglyceride levels in experimental animals and subjects with T2D [9, 10, 17, 34, 35]. Similar to PR-PFD, these agonists as gemfibrozil, including thiazolidinedione drugs, which are antidiabetic agents and ligands for Pparα and Pparγ activation, respectively, can enhance insulin sensitivity [9, 10, 17, 34, 35]. Gemfibrozil is used in clinical practice, but their utility is limited because just protect against CVDs in a modest fashion, and thiazolidinedione is used clinically to treat dyslipidemia and T2D [10]. In 2014, pirfenidone was recommended by the US Food and Drug Administration (FDA) for the treatment of idiopathic pulmonary fibrosis [36].

The cardioprotective and anti-fibrotic effects of PR-PFD in obese mice might be due to Pparα and Pparγ protein overexpression. Pparα and Pparγ activators attenuate cardiac fibrosis in T2D and hypertensive rats [37, 38]. Pparα is a lipid-sensitive receptor and drives the expression of Acox1 and Cpt1A, which are involved in the fatty acid β-oxidation. C57BL/6 J mice fed with HFD for 1 week exhibited increased Acox1 mRNA levels in the heart [33]. We also found an increase of Acox1 and Cpt1a protein expression in HFHC mice.

Pgc1a promotes fatty acid β-oxidation by functioning as a coactivator for Pparα and for others PPARs, and regulates mitochondrial biogenesis. The Pgc1a transcription is reduced in skeletal muscle and adipose cells of obese subjects; consistent with this, myocytes were treated with palmitate decreased Pgc1a expression [39]. Pgc1a overexpression on heart tissue led to an increase of Cpt1b mRNA levels and the expression of genes involved in oxidative phosphorylation [39].

Pparγ agonist rosiglitazone, an insulin-sensitizing drug, increased liver Pgc1a and Cpt1A proteins; meanwhile, Pparα agonist WY-14,643 increased Cpt1A and Acox1 proteins, when male Wistar rats were fed with low-fat standard chow diet by 12 days [40]. Both PPAR agonists decreased heart free fatty acids [40]. We also found in HFHC mice treated with PR-PFD a significant increase of Pgc1a mRNA levels and Acox1 and Cpt1A protein levels.

Mechanistically, Pparα and Pparγ agonists upregulate the heme-oxygenase (HO)-system, and its products such as carbon monoxide, bilirubin, biliverdin, and ferritin are implicated in the improvement of insulin sensitivity, lipid, and glucose metabolism, including inflammation and oxidative stress [12].

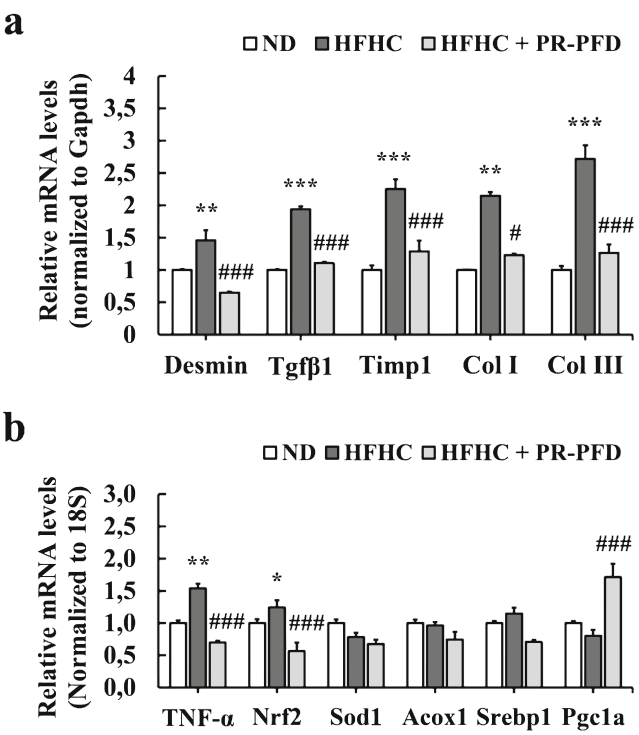

Fig. 6 Effects of HFHC diet and PR-PFD on the mRNA levels expression of genes in cardiac tissue. RT-qPCR for hypertrophy and fibrosis genes such as desmin, Tgfβ1, Timp1, Col I, and Col III (**a**); and for TNF-α, Nrf2, Sod1, Acox1, Srebp1, and Pgc1a (**b**) using ventricular tissue. Data are expressed in bar diagrams as mean ± SEM. For group comparisons (n = 5/group), one-way ANOVA followed by Tukey's post hoc analysis. *$P < 0.05$, **$P < 0.01$, and ***$P < 0.001$ vs. ND; $^{\#}P < 0.05$ and $^{\#\#\#}P < 0.001$ vs. HFHC

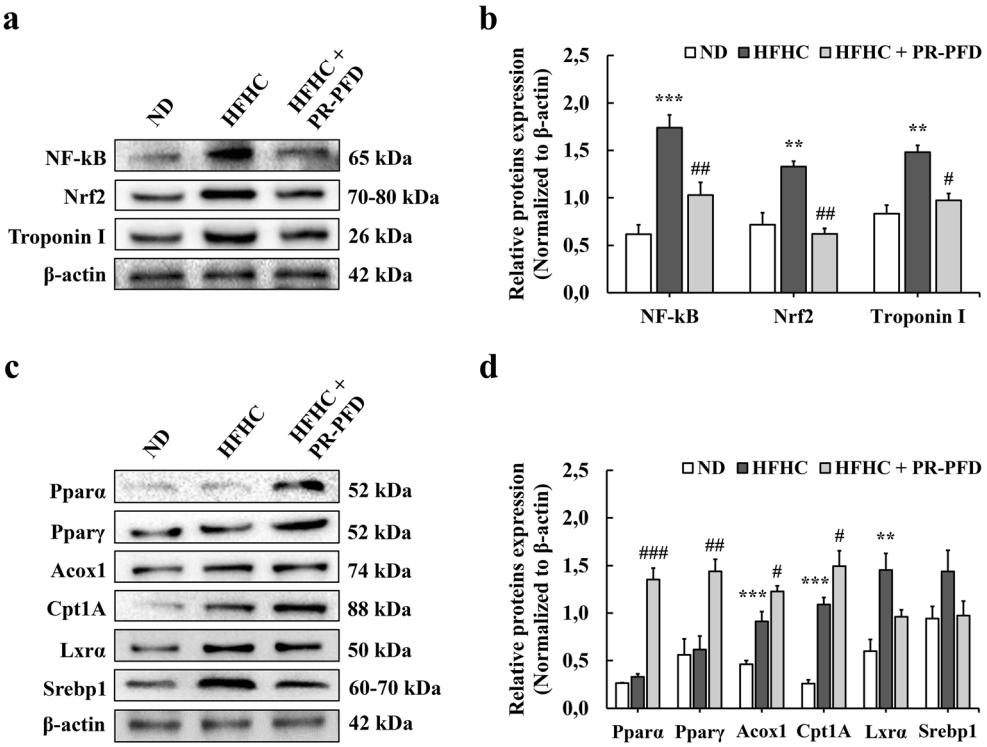

Fig. 7 Evaluation of inflammation, oxidative stress, myocardial damage, and lipid metabolism-related genes. Western blotting image and quantitation of NF-kB, Nrf2, troponin I (**a**, **b**); and Pparα, Pparγ, Acox1, Cpt1A, Lxrα, and Srebp1 (**c**, **d**) using cardiac protein extracts of ventricular tissue. Band intensities were measured and are shown in the histograms. Data are expressed as mean ± SEM. For group comparisons (n = 5/group), one-way ANOVA followed by Tukey's post hoc analysis. $^{**}P < 0.01$ and $^{***}P < 0.001$ vs. ND; $^{\#}P < 0.05$, $^{\#\#}P < 0.01$, and $^{\#\#\#}P < 0.001$ vs. HFHC

HO-1 is the inducible form, and improves insulin resistance and dyslipidemia in a mouse model of obesity [41]. HO-1 upregulates expression of Pgc1a to increase mitochondrial biogenesis, which inhibits fatty acids and adiposity [41]. Pparα and Pparγ induce transcriptionally to HO-1 by binding to PPAR responsive elements in the HO-1 gene; conversely,

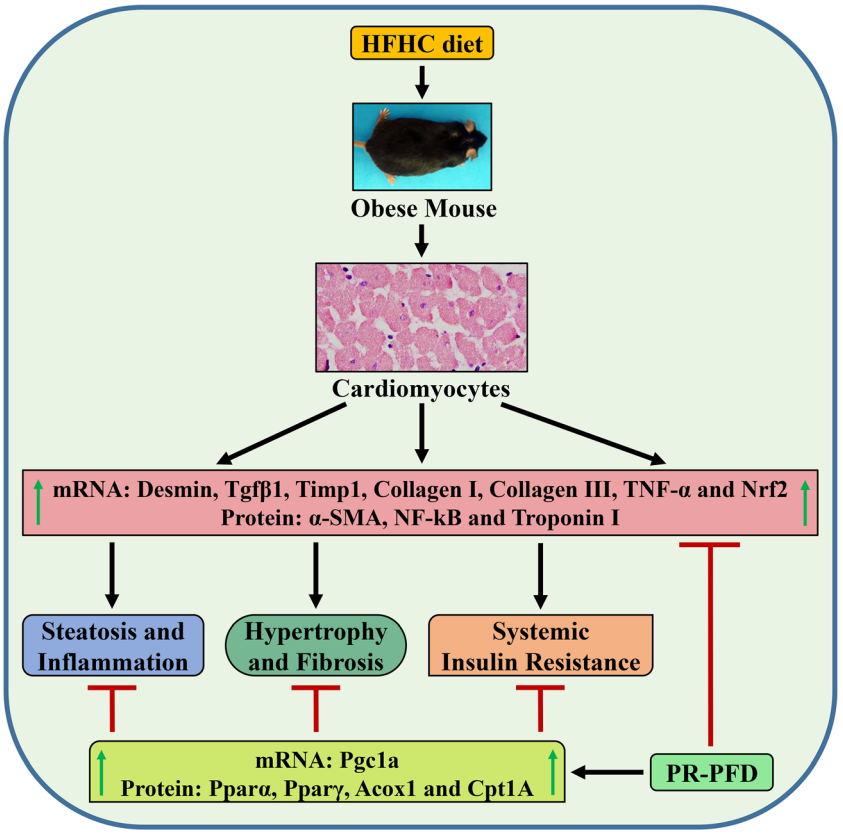

Fig. 8 Schematic diagram illustrating the potential cardioprotective effects of PR-PFD, which shows the Pparα, Pparγ, Acox1, and Cpt1A protein overexpression and prevents cardiac steatosis and inflammation as well as cardiac hypertrophy and fibrosis, including systemic insulin resistance induced by HFHC diet

the HO system potentiates Pparα and Pparγ effects [12]. Given that Pparα and Pparγ agonists are implicated in the lipid and carbohydrate metabolism, it is possible that HO-1 may be involved in the cardioprotective mechanism of PR-PFD to prevent cardiac steatosis and fibrosis in HFHC mice. Therefore, we considered to further analyze the PR-PFD effects on HO-1 in ventricular tissue of obese mice. Here, we have explored the effects of PR-PFD in the prevention and treatment of obesity-induced cardiac steatosis and fibrosis; a summary of the cardioprotective effect induced by PR-PFD is illustrated (Fig. 8). We need to further explore the mechanism of the effect of PR-PFD in obese mice model with heart-specific Pparα and Pparγ knockout animals.

Limitations

We acknowledge that the absence of data related to effects of PR-PFD on cardiac function and left ventricular wall thickness is a limitation of this study. Park et al. reported in C57BL/6 mice that ventricular fractional shortening declined significantly after 20 weeks of HFD compared with ND. Furthermore, the left ventricular posterior wall thickness at end-diastole was significantly increased in mice after 20 weeks of HFD compared with after 3 weeks of HFD, and it was not changed after 20 weeks of ND [6].

Conclusions

In summary, our data demonstrate for the first time that PR-PFD prevents cardiac steatosis in C57BL/6 J mice with obesity and NASH, improving insulin sensitivity, inflammation, cardiac hypertrophy, and fibrosis, including the upregulation of Pparα, Pparγ, Acox1, and Cpt1A genes. Our results give new insights into the cardioprotective effect of PR-PFD for the prevention and treatment of obesity-induced cardiac hypertrophy and fibrosis.

Authors' Contributions Dr. Jorge Gutiérrez-Cuevas contributed to experimental design, performed experiments, interpreted data, and wrote the manuscript. Dr. Ana Sandoval-Rodríguez and Dr. Monica Vazquez-Del Mercado contributed to experimental design. Dr. Hugo Christian Monroy-Ramírez and Dr. Arturo Santos-García contributed to critical intellectual input. Dr. Juan Armendáriz-Borunda contributed to experimental design and wrote the manuscript. All authors read and approved the final manuscript.

Funding Information This work was supported by the University of Guadalajara (PROSNI to JGC), by Fondo de Desarrollo Científico de Jalisco (FODECIJAL, project 8149-2019 to JGC, and project 7941-2019 to JAB) and by the Consejo Nacional de Ciencia y Tecnología (CONACYT, project 259096 to JAB).

Compliance with Ethical Standards

Conflict of Interest The authors declare that they have no conflict of interest. Dr. Juan Armendariz-Borunda is a consultant for Cell Pharma S.A. de C.V.

Ethical Approval All applicable international, national, and/or institutional guidelines for the care and use of animals were followed.

Informed Consent Not applicable.

References

1. Friedman JM. Modern science versus the stigma of obesity. Nat Med. 2004;10(6):563–9.
2. Organization WH: Obesity and overweight Web Site. https://www.who.int/news-room/fact-sheets/detail/obesity-and-overweight. Updated March 3, 2020. Accessed March 27, 2020.
3. Drosatos K, Schulze PC. Cardiac lipotoxicity: molecular pathways and therapeutic implications. Curr Heart Fail Rep. 2013;10(2):109–21.
4. Heydemann A. An overview of murine high fat diet as a model for Type 2 diabetes mellitus. J Diabetes Res. 2016;2016:2902351.
5. Kohli R, Kirby M, Xanthakos SA, Softic S, Feldstein AE, Saxena V, et al. High-fructose, medium chain trans fat diet induces liver fibrosis and elevates plasma coenzyme Q9 in a novel murine model of obesity and nonalcoholic steatohepatitis. Hepatology. 2010;52(3):934–44.
6. Park SY, Cho YR, Kim HJ, Higashimori T, Danton C, Lee MK, et al. Unraveling the temporal pattern of diet-induced insulin resistance in individual organs and cardiac dysfunction in C57BL/6 mice. Diabetes. 2005;54(12):3530–40.
7. Lavie CJ, Alpert MA, Arena R, Mehra MR, Milani RV, Ventura HO. Impact of obesity and the obesity paradox on prevalence and prognosis in heart failure. JACC Heart Fail. 2013;1(2):93–102.
8. Wang Z, Li L, Zhao H, Peng S, Zuo Z. Chronic high fat diet induces cardiac hypertrophy and fibrosis in mice. Metabolism. 2015;64(8):917–25.
9. Han L, Shen WJ, Bittner S, Kraemer FB, Azhar S. PPARs: regulators of metabolism and as therapeutic targets in cardiovascular disease. Part II: PPAR-beta/delta and PPAR-gamma. Futur Cardiol. 2017;13(3):279–96.
10. Han L, Shen WJ, Bittner S, Kraemer FB, Azhar S. PPARs: regulators of metabolism and as therapeutic targets in cardiovascular disease. Part I: PPAR-alpha. Future Cardiol. 2017;13(3):259–78.
11. Jia G, Hill MA, Sowers JR. Diabetic cardiomyopathy: an update of mechanisms contributing to this clinical entity. Circ Res. 2018;122(4):624–38.
12. Ndisang JF. Cross-talk between heme oxygenase and peroxisome proliferator-activated receptors in the regulation of physiological functions. Front Biosci (Landmark Ed). 2014;19:916–35.
13. Lopez-de la Mora DA, Sanchez-Roque C, Montoya-Buelna M, Sanchez-Enriquez S, Lucano-Landeros S, Macias-Barragan J, et al. Role and new insights of pirfenidone in fibrotic diseases. Int J Med Sci. 2015;12(11):840–7.
14. Avila G, Osornio-Garduno DS, Rios-Perez EB, Ramos-Mondragon R. Functional and structural impact of pirfenidone on the alterations of cardiac disease and diabetes mellitus. Cell Calcium. 2014;56(5):428–35.
15. Yamagami K, Oka T, Wang Q, Ishizu T, Lee JK, Miwa K, et al. Pirfenidone exhibits cardioprotective effects by regulating myocardial fibrosis and vascular permeability in pressure-overloaded hearts. Am J Physiol Heart Circ Physiol. 2015;309(3):H512–22.

16. Li C, Han R, Kang L, Wang J, Gao Y, Li Y, et al. Pirfenidone controls the feedback loop of the AT1R/p38 MAPK/renin-angiotensin system axis by regulating liver X receptor-alpha in myocardial infarction-induced cardiac fibrosis. Sci Rep. 2017;7:40523.
17. Sandoval-Rodriguez A, Monroy-Ramirez HC, Meza-Rios A, Garcia-Bañuelos J, Vera-Cruz J, Gutiérrez-Cuevas J, et al. Pirfenidone is an agonistic ligand for PPARα and improves NASH by activation of SIRT1/LKB1/pAMPK. Hepatol Commun. 2020;4(3):434–49.
18. Komiya C, Tanaka M, Tsuchiya K, Shimazu N, Mori K, Furuke S, et al. Antifibrotic effect of pirfenidone in a mouse model of human nonalcoholic steatohepatitis. Sci Rep. 2017;7:44754.
19. Dewey FE, Rosenthal D, Murphy DJ Jr, Froelicher VF, Ashley EA. Does size matter? Clinical applications of scaling cardiac size and function for body size. Circulation. 2008;117(17):2279–87.
20. Turner N, Kowalski GM, Leslie SJ, Risis S, Yang C, Lee-Young RS, et al. Distinct patterns of tissue-specific lipid accumulation during the induction of insulin resistance in mice by high-fat feeding. Diabetologia. 2013;56(7):1638–48.
21. Itani SI, Ruderman NB, Schmieder F, Boden G. Lipid-induced insulin resistance in human muscle is associated with changes in diacylglycerol, protein kinase C, and IkappaB-alpha. Diabetes. 2002;51(7):2005–11.
22. Ouwens DM, Boer C, Fodor M, de Galan P, Heine RJ, Maassen JA, et al. Cardiac dysfunction induced by high-fat diet is associated with altered myocardial insulin signalling in rats. Diabetologia. 2005;48(6):1229–37.
23. Chen G, Ni Y, Nagata N, Xu L, Zhuge F, Nagashimada M, et al. Pirfenidone prevents and reverses hepatic insulin resistance and steatohepatitis by polarizing M2 macrophages. Lab Investig. 2019;99(9):1335–48.
24. Dorn GW 2nd, Robbins J, Sugden PH. Phenotyping hypertrophy: eschew obfuscation. Circ Res. 2003;92(11):1171–5.
25. Park JH, Ku HJ, Kim JK, Park JW, Lee JH. Amelioration of high fructose-induced cardiac hypertrophy by naringin. Sci Rep. 2018;8(1):9464.
26. DeMartini T, Nowell M, James J, Williamson L, Lahni P, Shen H, et al. High fat diet-induced obesity increases myocardial injury and alters cardiac STAT3 signaling in mice after polymicrobial sepsis. Biochim Biophys Acta Mol Basis Dis. 2017;1863(10 Pt B):2654–60.
27. Takawale A, Zhang P, Patel VB, Wang X, Oudit G, Kassiri Z. Tissue inhibitor of matrix metalloproteinase-1 promotes myocardial fibrosis by mediating CD63-integrin beta1 interaction. Hypertension. 2017;69(6):1092–103.
28. Carlsen H, Haugen F, Zadelaar S, Kleemann R, Kooistra T, Drevon CA, et al. Diet-induced obesity increases NF-kappaB signaling in reporter mice. Genes Nutr. 2009;4(3):215–22.
29. Hommelberg PP, Plat J, Langen RC, Schols AM, Mensink RP. Fatty acid-induced NF-kappaB activation and insulin resistance in skeletal muscle are chain length dependent. Am J Physiol Endocrinol Metab. 2009;296(1):E114–20.
30. Riehle C, Abel ED. Insulin Signaling and Heart Failure. Circ Res. 2016;118(7):1151–69.
31. Grattendick KJ, Nakashima JM, Feng L, Giri SN, Margolin SB. Effects of three anti-TNF-alpha drugs: etanercept, infliximab and pirfenidone on release of TNF-alpha in medium and TNF-alpha associated with the cell in vitro. Int Immunopharmacol. 2008;8(5):679–87.
32. Choi YH, Back KO, Kim HJ, Lee SY, Kook KH. Pirfenidone attenuates IL-1beta-induced COX-2 and PGE2 production in orbital fibroblasts through suppression of NF-kappaB activity. Exp Eye Res. 2013;113:1–8.
33. Rindler PM, Plafker SM, Szweda LI, Kinter M. High dietary fat selectively increases catalase expression within cardiac mitochondria. J Biol Chem. 2013;288(3):1979–90.
34. Mussoni L, Mannucci L, Sirtori C, Pazzucconi F, Bonfardeci G, Cimminiello C, et al. Effects of gemfibrozil on insulin sensitivity and on haemostatic variables in hypertriglyceridemic patients. Atherosclerosis. 2000;148(2):397–406.
35. Verreth W, Ganame J, Mertens A, Bernar H, Herregods MC, Holvoet P. Peroxisome proliferator-activated receptor-alpha,gamma-agonist improves insulin sensitivity and prevents loss of left ventricular function in obese dyslipidemic mice. Arterioscler Thromb Vasc Biol. 2006;26(4):922–8.
36. Margaritopoulos GA, Vasarmidi E, Antoniou KM. Pirfenidone in the treatment of idiopathic pulmonary fibrosis: an evidence-based review of its place in therapy. Core Evid. 2016;11:11–22.
37. Ihm SH, Chang K, Kim HY, Baek SH, Youn HJ, Seung KB, et al. Peroxisome proliferator-activated receptor-gamma activation attenuates cardiac fibrosis in type 2 diabetic rats: the effect of rosiglitazone on myocardial expression of receptor for advanced glycation end products and of connective tissue growth factor. Basic Res Cardiol. 2010;105(3):399–407.
38. Ogata T, Miyauchi T, Sakai S, Takanashi M, Irukayama-Tomobe Y, Yamaguchi I. Myocardial fibrosis and diastolic dysfunction in deoxycorticosterone acetate-salt hypertensive rats is ameliorated by the peroxisome proliferator-activated receptor-alpha activator fenofibrate, partly by suppressing inflammatory responses associated with the nuclear factor-kappa-B pathway. J Am Coll Cardiol. 2004;43(8):1481–8.
39. Supruniuk E, Miklosz A, Chabowski A. The implication of PGC-1alpha on fatty acid transport across plasma and mitochondrial membranes in the insulin sensitive tissues. Front Physiol. 2017;8:923.
40. Strand E, Lysne V, Grinna ML, Bohov P, Svardal A, Nygard O, et al. Short-term activation of peroxisome proliferator-activated receptors alpha and gamma induces tissue-specific effects on lipid metabolism and fatty acid composition in male Wistar rats. PPAR Res. 2019;2019:8047627.
41. Drummond GS, Baum J, Greenberg M, Lewis D, Abraham NG. HO-1 overexpression and underexpression: clinical implications. Arch Biochem Biophys. 2019;673:108073.